ACS APPLIED MATERIALS & INTERFACES

Research Article

www.acsami.org

Synthesis and Characterization of Palladium and Palladium–Cobalt Nanoparticles on Vulcan XC-72R for the Oxygen Reduction Reaction

Lisandra Arroyo-Ramírez,[†] Rubenier Montano-Serrano,[†] Tatiana Luna-Pineda,[‡] Félix R. Román,[‡] Raphael G. Raptis,[†] and Carlos R. Cabrera*[,†]

[†]Department of Chemistry and NASA-URC Center for Advanced Nanoscale Materials, University of Puerto Rico, San Juan 00936-8377, Puerto Rico

[‡]Department of Chemistry, University of Puerto Rico, Mayagüez 00680, Puerto Rico

Supporting Information

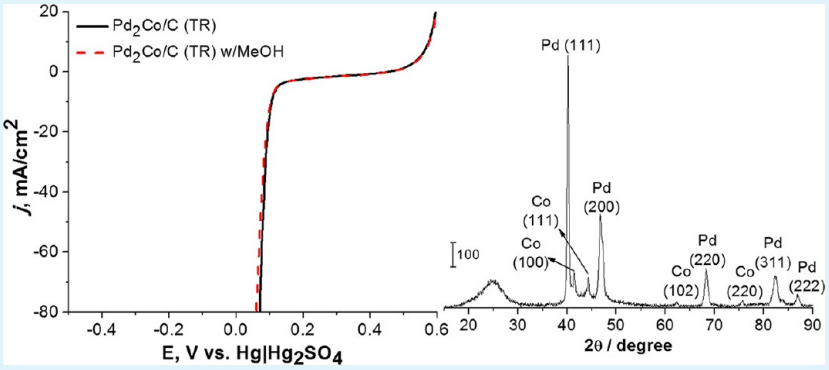

ABSTRACT: A single-source approach was used to synthesize bimetallic nanoparticles on a high-surface-area carbon-support surface. The synthesis of palladium and palladium–cobalt nanoparticles on carbon black (Vulcan XC-72R) by chemical and thermal reduction using organometallic complexes as precursors is described. The electrocatalysts studied were Pd/C, Pd_2Co/C, and $PdCo_2$/C. The nanoparticles composition and morphology were characterized using inductively coupled plasma mass spectrophotometer (ICP–MS), X-ray photoelectron spectroscopy (XPS), energy-dispersive X-ray fluorescence spectroscopy (EDS), X-ray diffraction (XRD), and transmission electron microscopy (TEM) techniques. Electrocatalytic activity towards the oxygen reduction reaction (ORR) and methanol tolerance in oxygen-saturated acid solution were determined. The bimetallic catalyst on carbon support synthetized by thermal reduction of the Pd_2Co precursor has ORR electrocatalytic activity and a higher methanol tolerance than a Pt/C catalyst.

KEYWORDS: *single precursor, Pd–Co alloy, bimetallic nanoparticles, ORR, methanol tolerant, direct methanol fuel cell*

INTRODUCTION

Proton-exchange membrane fuel cells (PEMFC) promise to be a power source for space application, transportation, stationary power, and portable devices with low or zero emissions and high efficiency.[1,2] One type of PEMFC is the direct methanol fuel cell (DMFC), which has the advantage of the fuel being liquid, allowing easy transportation and storage. Unfortunately, in the DMFC, the low-temperature electrolyte requires platinum (Pt) electrocatalysts that are easily poisoned and costly. Also, DMFCs suffer methanol crossover through the membrane that degrades the cathode catalysts. Platinum alloy- and non-Pt alloy-based catalysts were studied to reduce catalyst cost and to improve the catalytic activity toward the oxygen reduction reaction (ORR).[3−9] For example, the palladium–cobalt alloy resulted in being an extremely active catalyst for the ORR with high methanol tolerance.[10−14]

The support type, precursors used, and heat-treatment step are very important parameters to consider during the catalysts synthesis. The synthesis procedures for the catalysts are vital because the electrocatalysts performance will depend on them.[15] Various methods have been used for the electrocatalysts synthesis.[16−18] Chemical reduction of metal salts with a reducing agent is widely used for the synthesis of metallic and bimetallic nanoparticles on carbon supports.[19,20] Commonly, the alloys are prepared by deposition of a transition metal(1) and the catalyst metal(2) on the carbon support followed by the reduction process.[21,22] Simultaneous deposition and reduction of metals are used to avoid the problems of large particle sizes and difficult control of composition ratio. Serova et al. concluded that the selection of the precursor for the preparation of alloys can significantly affect the catalytic activity because differences in the catalysts morphology and electronic structure can be observed.[23] The electrocatalysts performance depends of the synthesis method. The demand for tailored

Received: July 20, 2013
Accepted: October 8, 2013
Published: October 8, 2013

catalytic nanoparticles has encouraged the use of heterobimetallic molecular precursors.[24−27] The advantage of the heterobimetallic molecular precursors for the synthesis of bimetallic and alloy nanoparticles is that the metal ratio is predetermined by the stoichiometry of the precursor.

This research focuses on the development of palladium and palladium−cobalt nanocatalysts on carbon support. The goal of this research is the synthesis of bimetallic catalytic nanoparticles using single organometallic precursors with the metal ratio predetermined. In this work, a simple synthesis of Pd, Pd_2Co, and $PdCo_2$ nanoparticles on Vulcan XC-27R has been accomplished. The morphology and composition of the carbon-supported catalysts were characterized by surface-analysis techniques. Electrochemical measurements have determined the electrocatalytic activity toward oxygen reduction reaction (ORR) and methanol tolerance.

EXPERIMENTAL SECTION

Synthesis of Nanoparticles on Vulcan XC-72R Using Organometallic Precursors. The organometallic complex $[Pd_3(\mu\text{-}3\text{-}PhPz)_6]$ (Pd_3 precursor), $[NH_4]_2[CoPd_2(Me_2Ipz)_4Cl_4]$ (Pd_2Co precursor), and $[NH_4]_2[Co_2Pd(Me_2Ipz)_4Cl_4]$ ($PdCo_2$ precursor) were synthesized following published procedures.[28,29] Carbon black (Vulcan XC-72R) from Cabot was used as the carbon support for the nanoparticles synthesis by chemical and thermal reduction. These synthesis methods were used with the Pd_3, Pd_2Co, and $PdCo_2$ precursors for the deposition of carbon-supported catalytic nanoparticles. For both methods, the catalysts were prepared, giving a total metal loading of 20 wt % (theoretical). All reagents and solvents were analytical grade and used as received.

The chemical reduction (CR) was carried out by mixing the precursor in 150 mL of tetrahydrofuran (THF, Aldrich) solvent with the Vulcan XC-72R (50 mg) under sonication for 30 min followed by stirring for 15 min. The reducing agent was 65 and 90 mg of sodium borohydride ($NaBH_4$, Aldrich) in 50 mL of THF for the palladium and palladium−cobalt precursors, respectively. After thoroughly dispersing the precursor in the Vulcan, an excess of reducing agent was slowly added drop by drop while stirring followed by further stirring for 2 h. Afterwards, the solution was filtered and washed copiously with deionized water. The sample was dried overnight at room temperature and then in air in an oven at 115 °C for 1 h. The heat treatment (or annealing step) was carried out at 600 °C under a N_2 atmosphere (CRht). The samples were labelled according to the precursor used as Pd/C (CRht), Pd_2Co/C (CRht), and $PdCo_2$/C (CRht), respectively.

The thermal reduction (TR) of the organometallic complex on Vulcan XC-72R was carried out as follows. The deposition of the precursors on Vulcan XC-72R was carried out by mixing the precursor in dichloromethane (CH_2Cl_2) solvent with Vulcan XC-72R under constant stirring for 30 min and sonication until the solvent evaporation. Then, the reduction process was performed in a closed-tube furnace by increasing the temperature to over 600 °C under a reductive hydrogen (H_2) atmosphere. The Pd, Pd_2Co, and $PdCo_2$ precursors in Vulcan were reduced at temperatures of over 620, 660, and 660 °C, respectively. The samples were labelled according to the precursor used as Pd/C (TR), Pd_2Co/C (TR), and $PdCo_2$/C (TR), respectively.

Physical Characterization. Surface-analysis techniques were used for the determination of the physical and chemical properties of the catalysts. The metal loading and the Pd and Co content in the catalyst samples was determined using an inductively coupled plasma-mass spectrophotometer (ICP−MS) from Agilent Technologies, model 7500ce. X-ray photoelectron spectroscopy (XPS) was used to determine the chemical composition of the nanocatalysts. A PHI 5600ci spectrometer with an Al Kα monochromatic X-ray source at 15 kV and 350.0 W was used to obtain a survey and multiplex XPS spectra. Spectra ware recorded at a take-off angle of 45° and a pass energy of 187.8 eV for the survey analysis and 58.7 eV for the high-energy resolution studies. The binding energies were corrected using the carbon (C 1s) contamination peak at 284.5 eV as a reference. The morphology of the nanoparticles was determined by electron microscopy techniques. A Carl Zeiss LEO-922 TEM microscope was used to obtain transmission electron microscopy images of the carbon-supported nanoparticles. Also, a FEI T12 Spirit TEM STEM with accelerating voltage of 120 kV was used to obtain the scanning transmission electron microscopy images. X-ray diffraction (XRD) patterns of the samples were measured by a Scintag Theta−Theta X-ray diffractometer using Cu Kα radiation (λ = 1.5406 Å) at scan rate of 0.60°/min.

Electrochemical Characterization. The electrochemical measurements were performed using an AutoLab (PGSTAT 30) potentiostat. A three-electrode cell was employed in all experiments, with a Pt spiral auxiliary electrode, and $Hg|Hg_2SO_4$ in K_2SO_4(satd) (0.64 V vs NHE) as the reference electrode. The catalyst ink was prepared by mixing 1 mg of catalyst, 250 μL of 2-propanol (Aldrich), and 8 μL Nafion® 5 wt % (Aldrich) followed by sonication for 1 h. Glassy carbon electrodes (3.0 mm dia., BASi) modified with the catalyst inks were used as working electrodes. First, glassy carbon electrodes (GCE) were polished mechanically with 1.0, 0.3, and 0.05 μm alumina (α-Al_2O_3) micropolishing (Buehler) until a mirrorlike surface was obtained followed by sonication in deionized water for 15 min to remove the alumina residues and then electrochemical polishing in 0.5 M H_2SO_4. Second, the GCE surface was modified with 8 μL of the catalysts ink mixture, and when it completely dried, the voltammetry was carried out. The Pd/C (TR), Pd/C (CRht), Pd_2Co/C (TR), Pd_2Co/C (CRht), $PdCo_2$/C (TR), and $PdCo_2$/C (CRht) catalysts were used. The commercial catalysts on carbon black used were 20% Pd/C (BASF), 20% Pt/C (Alfa Aesar), and 20% PtCo/C (1:1; BASF).

Cyclic voltammetry (CV) was carried out in a potential window between −0.65 and 0.90 V versus $Hg|Hg_2SO_4$ in 0.5 M H_2SO_4 at a scan rate of 100 mV/s. The potential window for Pt was −0.64 to 0.66 V versus $Hg|Hg_2SO_4$. The electroactive surface area (ESA) was determined by measuring the charge of the Pd oxide reduction region from the cyclic voltammetry in 0.5 M H_2SO_4 divided by the theoretical charge for a palladium oxide monolayer reduction (424 $\mu C/cm^2$).[30,31] For platinum, ESA was determined by measuring the charge of the Pt hydrogen desorption region from the cyclic voltammetry in 0.5 M H_2SO_4 divided by the theoretical charge of 210 $\mu C/cm^2$.[32,33] The mass activity (MA) was determined by dividing the current by the Pd mass in the ink. Linear sweep voltammetry (LSV) was done at potentials between 0.6 to −0.5 V versus $Hg|Hg_2SO_4$ in an oxygen saturated 0.5 M H_2SO_4 solution for 15 min at a scan rate of 5 mV/s. The study of the nanocatalysts tolerance toward methanol was done in 1.0 M MeOH in 0.5 M H_2SO_4 solution saturated with oxygen at a scan rate of 5 mV/s. All electrochemical experiments were carried out at room temperature. The deionized water used for the experiments was previously distilled and pumped through a Nanopure system (Barnstead) to give 18 MΩ cm resistivity.

RESULTS AND DISCUSSION

Characterization of the Pd/C Nanoparticles. The electrocatalysts synthesis was carried out by two synthetic routes: chemical and thermal reduction. The synthesis of the carbon-supported nanoparticles was carried out by the chemical reduction of the precursor in the Vulcan followed by annealing to form the catalytic nanoparticles. Another method used for the synthesis of the nanoparticles consisted of the deposition of the precursor in Vulcan followed by thermal reduction under H_2 to form the carbon-supported catalytic nanoparticles. Table 1 summarizes the metal loading and composition of the carbon-supported catalysts determined by inductively coupled plasma mass spectrometry (ICP−MS). The metal loadings determined by ICP−MS analyses were 16.9 and 15.2% for the Pd/C (CRht) and Pd/C (TR) catalysts, respectively.

Table 1. Determination of the Metal Content in the Carbon-Supported Catalysts Using Inductively Coupled Plasma Mass Spectrometry (ICP-MS) Analysis and the Crystalline Particle Size and Lattice Parameter of Pd/C, Pd_2Co/C, and $PdCo_2$/C Catalysts Synthesized by Chemical and Thermal Reduction from X-ray Diffraction Patterns

	ICP (% w/w)			crystallite size	lattice parameter
catalyst	Pd	Co	total	(nm)[a]	(nm)[a]
Pd/C (CRht)	16.90		16.90	3.9	0.3948
Pd/C (TR)	15.16		15.16	27	0.3898
Pd_2Co/C (CRht)	5.86	2.01	7.87	5.9	0.3794
Pd_2Co/C (TR)	7.27	4.45	11.72	25	0.3897
$PdCo_2$/C (CRht)	4.04	3.14	7.18	12	0.4024
$PdCo_2$/C (TR)	8.54	6.38	14.92	35	0.3865

[a]Crystallite size and lattice parameter were determined using the Pd (111) peaks.

The chemical composition characterization of the Pd_3 precursor on HOPG before and after thermal reduction using X-ray photoelectron spectroscopy (XPS) was previously reported.[34,35] The chemical composition of the catalytic nanoparticles on Vulcan XC-72R was also characterized by XPS. HR-XPS spectrum for Pd_3 precursor on Vulcan after chemical reduction (CR) shows the binding energies (BE) that correspond to the N (1s) peak and two doublet peaks assigned to Pd $3d_{5/2}$ and Pd $3d_{3/2}$ (Figure 1a). After heat treatment, the

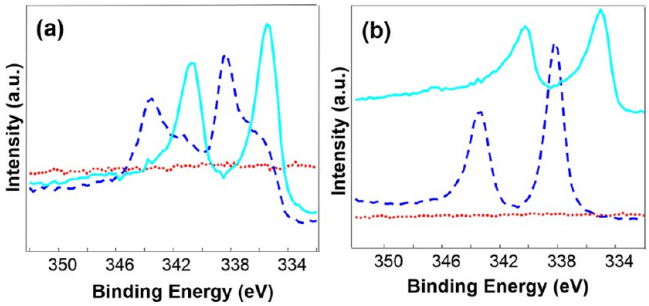

Figure 1. High-resolution XPS spectra for the Pd (3d) region in Vulcan XC-72R (dotted line). (a) Pd_3 precursor chemically reduced (dashed line) and after heat treatment (straight line) on Vulcan. (b) Pd_3 precursor deposited (dashed line) and thermally reduced (straight line) on Vulcan.

N (1s) signal vanishes and the Pd (3d) signal shifts to a lower BE (Figure 1a). The spectrum of the Pd_3 precursor deposited on Vulcan shows a N (1s) peak that disappears after the thermal-reduction process. After thermal reduction, a displacement toward lower BE for the Pd 3d peaks is observed (Figure 1b). The absence of the photoemission peak of the N (1s) in the XPS spectrum confirms the elimination of the organic functional group (pyrazolate). The binding-energy shifts provide information about the change of the oxidation state in palladium.

To obtain more information about the chemical composition and oxidation state, curve fitting of the spectra for Vulcan, Pd/C (CR), and Pd/C (CRht) was carried out. For Pd/C (CR), the O (1s) region has the smallest peak, with a BE of 531.0 eV for PdO.[36] The palladium oxide may have been generated during the catalyst drying process, which was carried out after filtration. In the Pd/C (CRht), the O (1s) region shows only the peak corresponding to the oxides in the carbon support. For Pd/C (CR), the Pd $3d_{5/2}$ region has peaks with BE values of 338.5, 336.8, and 335.5 eV, corresponding to Pd in the precursor, Pd oxide, and metallic Pd, respectively. In the Pd (3d) region for Pd/C (CRht), the peak corresponding to Pd in the precursor almost disappears, whereas the peak for Pd^0 (335.4 eV) has the highest intensity. The PdO peak (336.2 eV) can be the result of surface oxide and/or chemisorption of environmental oxygen.[37] From these results, it was determined that chemical reduction alone does not allow for the formation of metal nanoparticles and that the heat treatment is necessary to completely eliminate the pyrazolate ligands of the precursor and to form Pd nanoparticles on Vulcan.

The curve-fitted HR-XPS spectrum for the Pd (3d) region for the Pd_3 precursor deposited on Vulcan shows a peak at a BE value of 338.6 eV that corresponds to Pd^{2+} in the pyrazolate. For the Pd/C (TR) catalysts, the Pd (3d) region contains three peaks corresponding to the metallic Pd (335.3 eV), PdO (336.3 eV), and PdO_2 (337.9 eV). The binding-energy displacement of 3.3 eV toward lower a BE in the Pd region shows the change of the oxidation state and demonstrates that the composition of the modified Vulcan surface changes after the reduction process. The palladium oxide formation can be explained by different effects: during the cooling process, oxygen diffused out of the Vulcan, or atmospheric oxygen was chemisorbed when the furnace was opened at 30 °C. The thermal-reduction process under H_2 removes the ligands and promotes the formation of the Pd metallic nanoparticles on Vulcan.

Transmission electron microscopy images for the chemically reduced palladium precursor show nanoparticles with good distribution through the carbon surfaces and an average size of (2.3 ± 1.1) nm. After the heat treatment, these particles grow to (3.3 ± 1.2) nm (Figure 2). In the literature, Pd/C

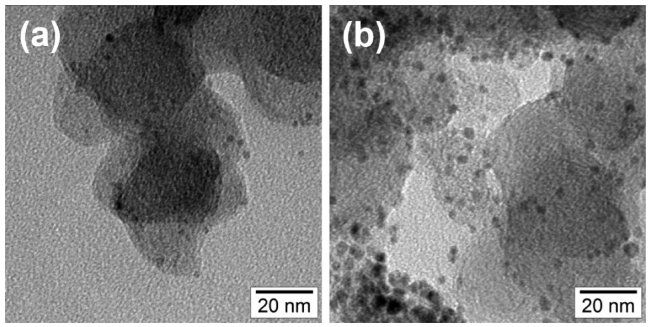

Figure 2. Transmission electron microscopy (TEM) images for the (a) Pd/C (CR) and (b) Pd/C (CRht) catalysts.

nanoparticles with a particle size range from 4.5 to 7.5 nm, formed by the polyol process, have been reported.[38] In TEM images for the thermally reduced Pd_3 precursor, the average particles size was (24 ± 11) nm (Figure 3).

X-ray diffraction (XRD) analysis was used for the phase identification of the crystalline catalyst and for the determination of its average particle size. The palladium carbon-supported catalyst has a face-centered cubic (fcc) structure, and the Pd (111) plane was used to determine the crystalline particle size and lattice parameter. The diffraction pattern for the Pd/C (CR) shows broad peaks at 2θ angles of 24.6° and 39.8°, corresponding to carbon (Vulcan) and the Pd (111) plane, respectively (see Figure S1a in the Supporting Information). The position of the Pd (111) plane is at a 2θ

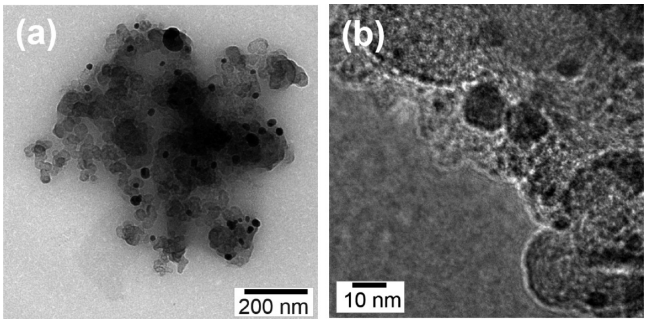

Figure 3. Transmission electron microscopy (TEM) images for the Pd/C (TR) catalyst.

angle of 40.1°, and the corresponding lattice parameter (a_o) is 0.3890 nm, according to the power diffraction database.[39] The peak at the 2θ angle of 39.5° corresponding to the Pd (111) plane becomes narrower after the heat treatment (Pd/C (CRht)). More crystalline nanoparticles were obtained after the heat-treatment process. Figure S1b shows the X-ray diffraction patterns for Pd/C catalysts synthesized by thermal reduction. The diffraction pattern consists of five peaks at 40.0°, 46.5°, 68.0°, 82.0°, and 86.5° for Pd planes (111), (200), (220), (311), and (222), respectively. The peaks for Pd/C (TR) are narrower and more intense than the peaks for the Pd/C (CRht). The particle sizes in the catalysts can be calculated with the Scherrer equation using the Pd (111) peak.[21,40] For Pd/C (CR), the particles are amorphous and change to crystalline after the heat treatment under nitrogen. In the Pd catalysts synthesized by thermal reduction, the particles were crystalline. The crystallite size for Pd/C (CRht) and Pd (TR) is 3.9 and 27 nm, respectively. Pd/C (CRht) has a particle size similar to those determined by TEM. The crystallite size is bigger for the Pd/C (TR) catalysts, and the lattice parameter is closer to the Pd standard value. Table 1 summarizes the results of the X-ray diffraction analysis for the crystallite size and lattice parameter for the catalysts synthesized by chemical and thermal reduction.

Characterization of the Pd_2Co/C Nanoparticles. The bimetallic nanoparticles synthesis on Vulcan was carried out using a single precursor with the palladium−cobalt ratio (2:1 or 1:2) predetermined. In this section, the characterization by surface-analysis techniques of the Pd_2Co/C catalytic nanoparticles synthesized by chemical reduction and thermal reduction of the Pd_2Co precursor will be discussed. The ICP−MS analyses presented a total metals loading of 7.9 and 11.7% for Pd_2Co/C (CRht) and Pd_2Co/C (TR) catalysts, respectively. The metal loading obtained by ICP−MS analysis was lower than expected. The Pd/Co metal ratio was 2:1 in the precursor. From Table 1, the metal ratios (Pd/Co) were 2.9:1 for Pd_2Co/C (CRht) and 1.6:1 for Pd_2Co/C (TR) from ICP−MS analysis. For Pd_2Co/C (TR), the metal ratio is closer to the organometallic precursor.

The XPS spectrum for Pd_2Co/C (CR) shows the photoemission peaks at BE values corresponding to Pd (3d), Co (2p), C (1s), O (1s), I (3d), and N (1s). The peak at BE corresponding to the Cl (2p) atom is not present. The chemical reduction eliminates the chloride ligand but not the pyrazolates. As in the Pd_3 precursor, heat treatment is necessary for the complete metallic nanoparticles formation. Figure 4 shows the HR-XPS spectra for the regions of Pd, Co, I, and N of the Vulcan (red), the chemically reduced Pd_2Co precursor (blue),

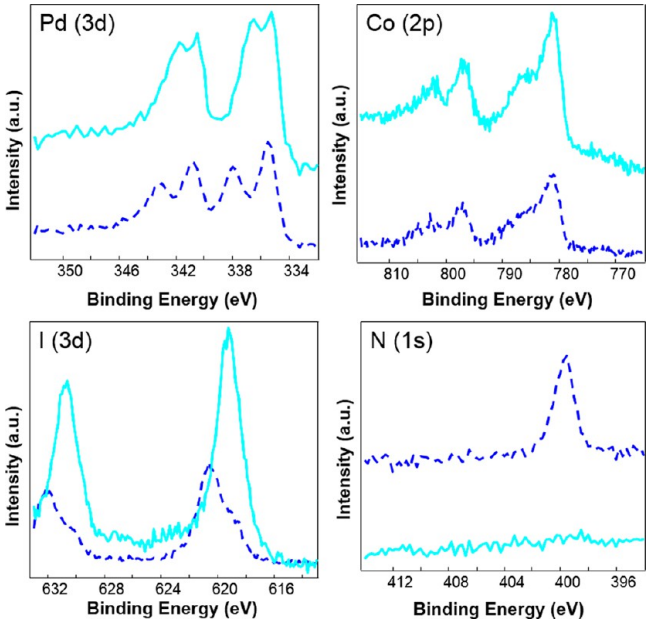

Figure 4. High-resolution XPS spectra for the Pd (3d), Co (2p), I (3d), and N (1s) regions in the chemically reduced Pd_2Co precursor (dashed line) and after heat treatment (straight line) on Vulcan.

and after heat treatment (cyan) on Vulcan. In the HR-XPS for the I (3d) region, it was observed that the peaks have a displacement of BE after heat treatment but do not disappear (Figure 4). The N and Cl peaks disappear after the heat treatment. The Pd $3d_{5/2}$ region in Pd_2Co/C (CR) has two peaks, and after the heat treatment they have a displacement to a lower BE.

Table S1 presents the results for the BE values obtained from HR-XPS curve-fitting studies for the Pd_2Co precursor chemically reduced and after heat treatment on Vulcan XC-72R. The peaks at BE values of 335.6 and 337.9 eV can be attributed to Pd^0 and Pd^{+2}, respectively. For the Co $2p_{3/2}$ region, the peak with BE of 781.2 eV and a shakeup satellite peak at 786.4 eV are attributed to cobalt in the precursor.[41] Pd_2Co/C (CRht) has BE at 335.7, 337.0, and 338.9 eV for Pd $3d_{5/2}$ that can be attributed to Pd^0 and Pd^{+2}. The literature reports BE values of 335.1 eV for metallic Pd,[42] 335.7 eV for PdCo alloy,[43−45] 337.9 eV for PdO_2, and 339.0 eV for Pd^{2+}.[42] In the Co (2p) region, the peak at 781.8 eV has a higher BE than metallic cobalt[42] and can be attributed to cobalt-containing bimetallic alloy because of its similarity to the reported value of 781.9 eV for PtCo.[46]

The XPS spectrum for the Pd_2Co precursor on Vulcan shows the characteristic element peaks for the complex (Pd, Co, C, N, I, and Cl) and for the carbon support (C and O elements). After thermal reduction, the Pd and Co peaks from the complex and the C and O peaks from the support are the only ones remaining. The thermal-reduction process completely eliminates the ligands and forms the Pd_2Co/C catalytic nanoparticles, contrary to the chemical reduction with heat treatment process.

Table S1 lists the BE values obtained from the HR-XPS spectral curve fitting for the Pd_2Co precursor deposited on Vulcan and Pd_2Co/C (TR) catalysts. The Pd (3d) region clearly shows a shift to lower BE, which demonstrates the change in the chemical environment and the oxidation state of the palladium The BE values at 338.2 and 339.3 eV can be attributed to the two species at the precursor. A BE value of

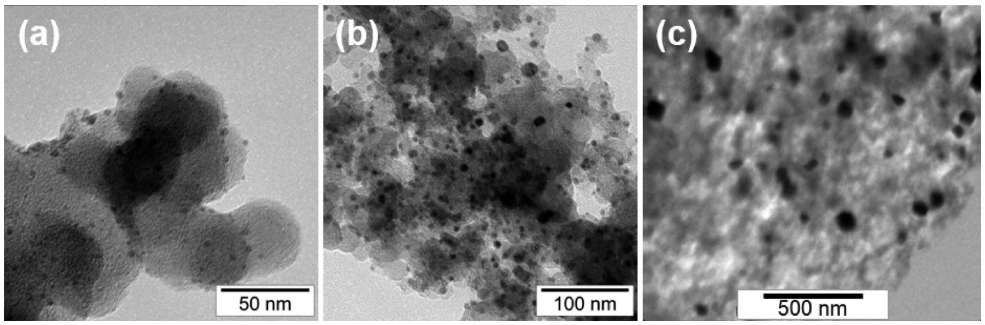

Figure 5. Transmission electron microscopy (TEM) images for the (a) Pd_2Co/C (CR) and (b) Pd_2Co/C (CRht) catalysts. (c) Scanning transmission electron microscopy (STEM) images for the Pd_2Co/C (TR) catalyst.

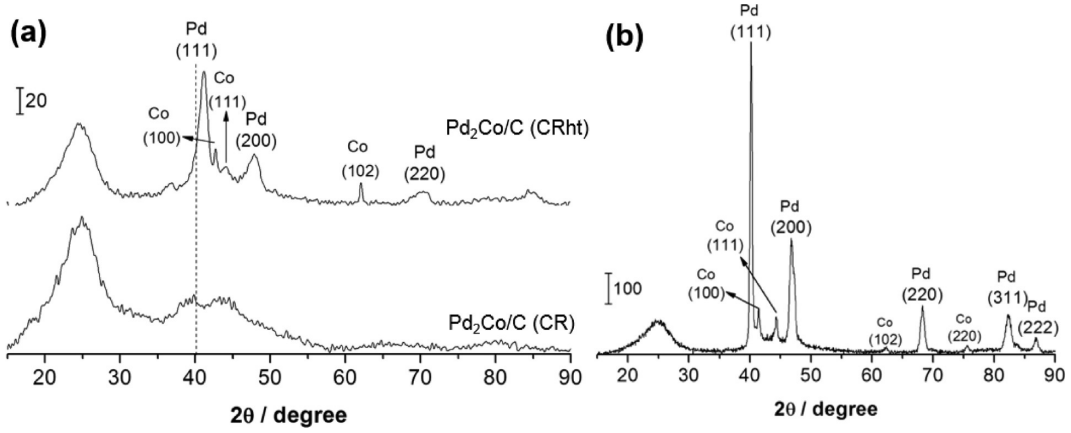

Figure 6. X-ray diffraction patterns for the Pd_2Co/C catalysts synthesized by (a) chemical reduction and (b) thermal reduction of the Pd_2Co precursor on Vulcan.

338.4 eV was reported for the Pd_2Co precursor on HOPG surface.[47] The peak at a BE of 335.7 eV for the Pd^0 and 338.4 eV for the Pd^{2+} oxidation state was observed in the Pd_2Co/C (TR) catalyst. For Pd alloy, the shift to a higher BE in the d-band of Pd is due to the d−d band hybridization upon alloying with Co.[43,48] This shift indicates a decrease in the density of states at the Fermi level, which might weaken the chemisorption of O and OH on the Pd sites and could enhance of the ORR activity.[43] In the Co $2p_{3/2}$ region, the peak with a BE of 781.6 eV and a shakeup satellite peak at 786.9 eV are attributed to cobalt in the precursor. After thermal reduction, the peak at BE value of 781.8 eV can correspond to Co^0 for the formation of the alloy with palladium, as discussed above.

Figure 5a,b shows TEM images for the Pd_2Co precursor chemically reduced and after heat treatment. These images show a good distribution of the nanoparticles throughout the carbon support and an average size of (2.6 ± 1.3) nm. After the heat treatment, these particles grow to (6.0 ± 3.1) nm. The thermal reduction of the Pd_2Co precursor gives bigger particles than the chemical reduction (Figure 5c). The Pd_2Co/C (TR) catalysts have an average particle size of (62 ± 21) nm. Particles synthesized by thermal reduction tend to agglomerate, and the particle sizes are larger. The average particle sizes of the Pd_2Co/C catalysts were larger than Pd/C catalysts, as expected. In the literature, it has been reported that the bimetallic nanoparticles have a tendency to agglomerate.[49] STEM/EDS map line scans of Pd_2Co/C (TR) catalysts show that the nanoparticle is composed of the elements palladium and cobalt (Figure S2). The nanoparticle is bimetallic and is not an oxide of the metals. Also, SEM/EDS mapping images for the Pd, Co, and C elements show the composition and metal distribution of the $PdCo_2/C$ (TR) catalyst (Figure S3). The literature explains that homogeneous alloys on the surface of a metal with a high negative free energy for oxide formation (Co) and a metal with high standard reduction potential (Pd) can increase the ORR catalytic activity.[12,50]

XRD analysis for the chemically reduced Pd_2Co precursor shows that the amorphous particles will crystallize after the heat treatment under nitrogen, as occurs with the Pd_3 precursor (Figure 6a). Table 1 summarizes the results of the lattice parameters obtained for the catalysts. The diffraction pattern for the chemical reduction of the Pd_2Co precursor on Vulcan shows broad peaks at 24.7°, 38.9°, and 44.3°, corresponding to carbon and the Pd (111) and Co (111) planes, respectively. The peak narrowed and new peaks appeared after the heat treatment. The Pd reflections were shifted to a higher 2θ angle value because of the substitution with smaller Co atoms and the formation of alloyed particles.[49,51] Figure 6b shows the X-ray diffraction patterns for Pd_2Co/C catalysts synthesized by thermal reduction. The lattice parameter for Pd_2Co (TR) (a_o = 0.3897 nm) is slightly higher than that for palladium (0.3890 nm) and can be attributed to alloy formation.[52] The crystalline particle sizes for Pd_2Co/C (CRht) and Pd_2Co (TR) were 5.9 and 25 nm, respectively. The crystalline size is bigger for thermal reduction, and the lattice parameter value is very close to the Pd/C (TR) catalysts (Table 1). The particle size for Pd_2Co/C (CRht) is similar to that determined by TEM.

Characterization of the $PdCo_2/C$ Nanoparticles. The metal loadings, determined by ICP−MS analysis, were 7.18%

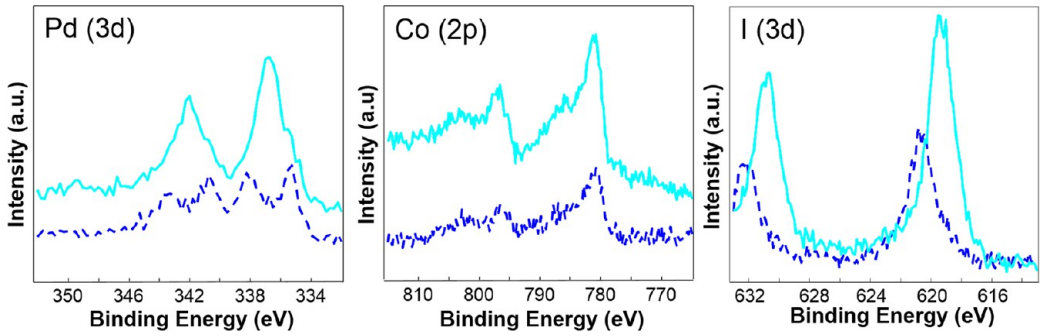

Figure 7. High-resolution XPS spectra for the Pd (3d), Co (2p), and I (3d) signals in the chemically reduced $PdCo_2$ precursor (dashed line) and after heat treatment (straight line) on Vulcan.

for $PdCo_2$/C (CRht) and 14.9% for $PdCo_2$/C (TR) catalysts. The Pd/Co ratio was 1.3:1 for $PdCo_2$/C (CRht) and Pd_2Co/C (TR) catalysts (Table 1). These results do not match the expected metal ratio of the precursor. From the XPS atomic percent, $Pd_{39}Co_{61}$ and $Pd_{51}Co_{49}$ stoichiometries were obtained for the catalysts synthesized by chemical reduction and thermal reduction, respectively. From the XPS analysis, the carbon-supported catalyst synthesized by chemical reduction was obtained with the metals ratio close to those of the precursor.

The XPS spectrum for $PdCo_2$/C (CR) shows BE for the Pd (3d), Co (2p), C (1s), O (1s), and I (3d) peaks but not for the Cl (2p) and N (1s) peaks. After the heat treatment, the Pd, Co, C, O, and I peaks shifted to lower BE values (Figure 7). In the $PdCo_2$/C (CRht), the I (3d) peak remained after the heat treatment, showing the same behavior as in the Pd_2Co/C (CRht). It is not understood why peak I remains after the heat treatment, whereas the pyrazolate ligand (N peak) disappears. Table S2 summarizes the results of the values obtained from HR-XPS curve fitting for the chemically reduced $PdCo_2$ precursor and after heat treatment as well as of the $PdCo_2$ precursor deposited and after thermal reduction on Vulcan XC-72R. For $PdCo_2$/C (CR), the Pd $3d_{5/2}$ region shows two peaks at BE values of 335.6 and 338.3 eV, corresponding to the metallic Pd and Pd^{2+} in the precursor, respectively. For Co $2p_{3/2}$, the peaks at BE values of 781.5 and 786.0 eV can be attributed to cobalt in the precursor and a shakeup satellite peak, respectively. For the $PdCo_2$/C (CRht) catalysts, in the Pd (3d) region the peaks at BE of 335.6 (Pd^0) and 338.3 eV (Pd–N) have a lower intensity than the new peak at 337.1 eV attributed to Pd oxides. In the Co (2p) region, a BE shift is not observed for the peak corresponding to cobalt in the precursor. The $PdCo_2$ precursor has a peak at a BE value of 781.6 eV for the Co $2p_{3/2}$ signal, and the literature reports a BE value of 781.9 eV for Co $2p_{3/2}$ in PtCo alloy.[46] Because of the results discussed above for the cobalt region in the $PdCo_2$/C (CRht), it is difficult to determine if the chemical-reduction process reduced Co^{+2} to Co^0.

After thermal reduction of the $PdCo_2$ precursor deposited on Vulcan, the characteristic peaks for I, Cl, and N disappear, and only the Pd and Co peaks (from the complex) and the C and O peaks (from the support) remained. Table S2 presents the BE values obtained for the $PdCo_2$/C (TR) catalysts. For the Pd $3d_{5/2}$ region, the peaks at BE values of 335.8 eV can be attributed to metallic Pd or bimetallic Pd,[53] and the peak at 338.5 eV can be attributed to the Pd–N in the precursor. The XRD data discussed below present a decrease in the lattice dimensions compared with pure Pd, which can be attributed to the formation of PdCo alloy. For the Co $2p_{3/2}$ region, the peak at a BE value of 780.8 eV corresponds to metallic cobalt.

Figure 8 shows the electron microscopy images for the $PdCo_2$/C (CRht) and $PdCo_2$/C (TR) catalysts. The particles

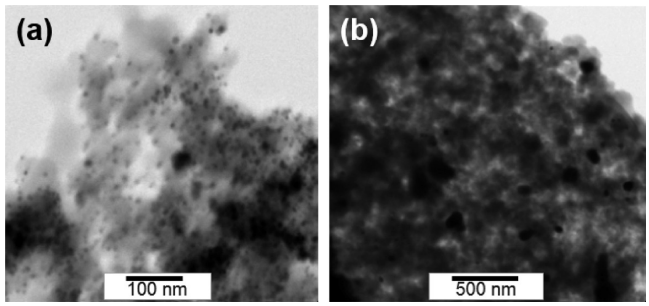

Figure 8. Scanning transmission electron microscopy (STEM) images for the (a) $PdCo_2$/C (CRht) and (b) $PdCo_2$/C (TR) catalysts.

size was between 2.6 and 22 nm for $PdCo_2$/C (CRht). Thermal reduction of the $PdCo_2$ precursor produced larger particles with particles sizes between 29 and 309 nm (Figure 8b). Average particle sizes of (9.1 ± 4.9) nm for $PdCo_2$/C (CRht) and (138 ± 75) nm for $PdCo_2$/C (TR) were determined. For both synthetic methods, chemical and thermal reduction, the particles sizes for the $PdCo_2$/C catalysts were bigger than those of the Pd/C and Pd_2Co/C catalysts. The nanoparticles synthesis by chemical reduction results in a more homogeneous particle-size distribution when compared with the thermal-reduction process. Optimizations of the catalyst's synthesis by thermal reduction of the precursor is needed if a more homogeneous particle distribution is desired and/or to obtain smaller nanoparticles.

The X-ray diffraction pattern for $PdCo_2$/C (CR) and $PdCo_2$/C (CRht) shows broad peaks that make them difficult to assign to their corresponding planes (Figure S4a). $PdCo_2$/C (TR) has a similar crystal structure as Pd_2Co/C (TR), as shown in Figure S4b. For $PdCo_2$/C (TR), the lattice parameter is lower than for Pd because of the increase in the cobalt content. The crystalline particle sizes for $PdCo_2$/C (CRht) and $PdCo_2$/C (TR) are 12 and 35 nm, respectively. The lattice parameter value for the $PdCo_2$/C (TR) was smaller than the values for the Pd/C (TR) and Pd_2Co/C (TR) catalysts (Table 1) and can be attributed to the formation of the alloy. This contraction of the lattice was expected for the incorporation of the smaller Co atoms in the Pd fcc structure.[49]

Electrochemical Characterization. Cyclic voltammetry (CV) was used to study the electrochemical behavior of the

bare glassy carbon electrode and the Pd/C, Pd_2Co/C, and $PdCo_2$/C nanocatalysts synthesized by chemical and thermal reduction (Figure 9). Figure 9a shows the cyclic voltammo-

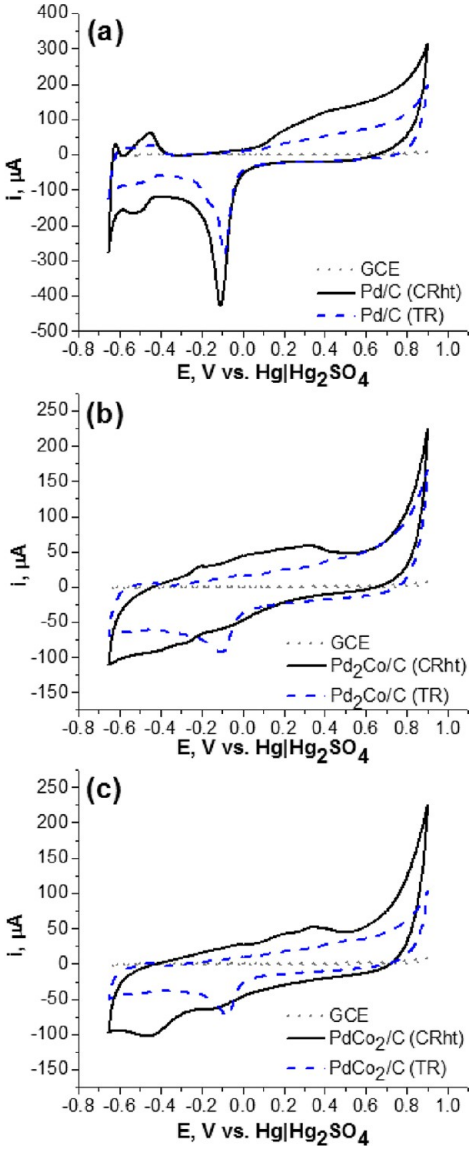

Figure 9. Cyclic voltammograms for the bare glassy carbon electrode (dotted line) and (a) Pd/C, (b) Pd_2Co/C, and (c) $PdCo_2$/C catalysts synthesized by chemical (straight line) and thermal (dashed line) reduction in 0.5 M H_2SO_4. Scan rate = 100 mV/s.

grams for the Pd/C catalysts synthesized by chemical (straight line) and thermal (dash line) reduction of the Pd_3 precursor on Vulcan. Pd/C (CRht) has a lower current in the Pd oxide reduction and hydrogen ad/desorption regions than Pd/C (TR). The Pd oxide reduction peak for the Pd/C (TR) has a negative shift of 19 mV compared to Pd/C (CRht). Figure 9b shows the cyclic voltammograms for the Pd_2Co/C catalysts synthesized by chemical and thermal reduction of the Pd_2Co precursor on Vulcan. The Pd_2Co/C (CRht) catalyst does not have Pd oxide reduction and hydrogen ad/desorption peaks. This is expected because in the XPS analysis traces of iodine from the precursor was found. Pd_2Co/C (TR) showed Pd oxide reduction but not peaks for the hydrogen region. The cobalt in the catalysts can be the reason that the peaks in the hydrogen region do not appear. Tominaka et al. point out that alloying Pd with Co inhibits hydrogen absorption into the Pd–Co catalyst.[54] Similar voltammograms were obtained with the $PdCo_2$/C catalysts synthesized by chemical and thermal reduction of the $PdCo_2$ precursor on Vulcan (Figure 9c). Table 2 presents the charges and the electrochemical surface

Table 2. Cathodic Current Density and Mass Activity for the Oxygen Reduction Reaction at 0.100 V vs $Hg|Hg_2SO_4$ in 0.5 M H_2SO_4 and Electrochemical Charge and Calculated Electrochemical Surface Area for the Catalytic Nanoparticles

electrocatalysts	current density $(A/cm^2)^a$	mass activity $(A/mg_M)^a$	charge $(\mu C)^b$	surface area $(cm^2)^c$
Pd/C (CRht)	-7.45×10^{-6}	-1.38×10^{-3}	411	0.968
Pd/C (TR)	-4.65×10^{-5}	-5.79×10^{-3}	248	0.585
Pd_2Co/C (CRht)				
Pd_2Co/C (TR)	-1.45×10^{-5}	-1.55×10^{-3}	102	0.240
$PdCo_2$/C (CRht)				
$PdCo_2$/C (TR)	-1.22×10^{-5}	-8.75×10^{-4}	80.9	0.191
Pd/C commercial	-9.67×10^{-6}	-4.17×10^{-3}	1117	2.634
Pt/C commercial	-1.47×10^{-4}	-1.37×10^{-2}	116	0.551
PtCo/C commercial	-1.84×10^{-4}	-2.75×10^{-2}	95.6	0.455

[a]Cathodic current density and mass activity for the oxygen reduction reaction at 0.100 V vs $Hg|Hg_2SO_4$. For ORR activity, the solution was purged with oxygen for 15 min before each experiment. [b]Electrochemical charge of the palladium surface oxide reduction and platinum hydrogen desorption. [c]Electrochemical surface areas were calculated from the electrochemical palladium surface oxide reduction charge and a conversion factor of 424 $\mu C\ cm^{-2}$. For platinum, electrochemical surface areas were calculated from the hydrogen desorption charge and a conversion factor of 210 $\mu C\ cm^{-2}$.

areas (ESA) determined for the catalysts. A greater electrochemical surface area translates to more active sites for carrying out the catalytic activity. The Pd/C (CRht) nanocatalyst has a smaller particle size and larger electrochemical surface area.

Linear sweep voltammetry (LSV) in acidic solution saturated with oxygen was used to determine the catalytic activity toward the oxygen reduction reaction (ORR). Figure 10 shows the linear sweep voltammograms for the Pd/C, Pd_2Co/C, and $PdCo_2$/C nanocatalysts synthesized by chemical and thermal reduction in a 0.5 M H_2SO_4 and 1.0 M MeOH/0.5 M H_2SO_4 solution saturated with oxygen at 5 mV/s. Figure 10a shows that Pd/C (CRht) has similar ORR activity as the Pd/C (TR) catalyst. Pd/C (TR) has a positive onset potential of 25 mV at a current of −20 μA compared with Pd/C (CRht). This result was not expected because the Pd/C (CRht) has the smallest particle size and therefore more surface area and should have a greater catalytic activity. Figure 10b,c shows that Pd_2Co/C (CRht) and $PdCo_2$/C (CRht) have poor ORR activity. The crystalline size and the alloy degree can affect the ORR activity.[12] As discussed above, these catalysts have iodine residues that can be the reason for the low ORR electrocatalytic activity. The oxygen reduction reaction in Pd_2Co/C (TR) has a positive onset potential of 12 mV when compared with PdCo2/C (TR). From LSV, similar ORR activity with and without methanol is observed. The only difference in the ORR activities

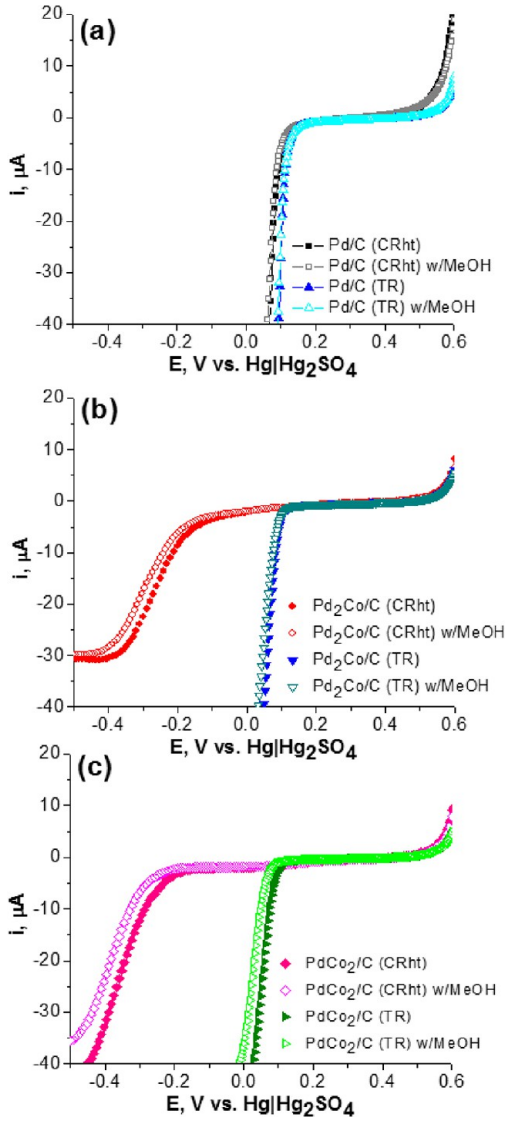

Figure 10. Linear sweep voltammograms for the catalysts synthesized by chemical (CRht) and thermal (TR) reduction without (filled symbols) and with a 1 M MeOH in 0.5 M H_2SO_4 (open symbols) solution purged with oxygen for 15 min before each experiment: (a) Pd/C (CRht) (square) and Pd/C (TR) (triangle), (b) Pd_2Co/C (CRht) (circle) and Pd_2Co/C (TR) (triangle down), and (c) $PdCo_2$/C (CRht) (diamond) and $PdCo_2$/C (TR) (triangle right). Scan rate = 5 mV/s.

with methanol for the Pd_2Co/C and $PdCo_2$/C catalysts is that they have a negative potential shift of only a few millivolts. The commercial Pd/C, Pt/C, and PtCo/C catalysts were used to compare the ORR activity and methanol tolerance to that of our catalysts (see Figure S5 in the Supporting Information). The Pd/C commercial catalyst has negative potential shifts when compared with the Pt/C and PtCo/C commercial catalysts. The Pd/C catalyst has no potential loss in comparison with the Pt/C and PtCo/C catalysts in the presence of MeOH. Pt/C and PtCo/C have higher ORR activity but the lowest methanol tolerance. It is well known that Pd is used for alcohol electrooxidation in alkaline media, but alcohol electrooxidation in acidic solutions does not occur.[55] The MeOH crossover from the anode to the cathode causes cell voltage loss in the DMFC. This is why it is important to find non-Pt-based catalysts with excellent methanol tolerance. The high methanol tolerance of the palladium catalysts in acid media was confirmed. Our palladium-based nanocatalysts have higher methanol tolerance than the platinum and platinum−cobalt commercial catalysts.

Table 3 summarizes the ORR onset potential for our Pd/C, Pd_2Co/C, and $PdCo_2$/C nanocatalysts as well as the commercial Pt/C, PtCo/C, and Pd/C at a current density of $-20\ \mu A/cm^2$ and a mass activity of $-2\ mA/mg_M$. The trend from the best to worst catalyst is: Pt/C (commercial) > PtCo/C (commercial) > Pd/C (TR) > Pd_2Co/C (TR) > $PdCo_2Co$/C (TR) > Pd/C (commercial) when ORR activity has a current normalized by the electrochemical surface area (Figure 11a). These results demonstrate that our Pd/C, Pd_2Co/C, and $PdCo_2$/C catalysts synthesized by thermal reduction have better ORR activity than commercial Pd/C. Figure 11b shows that the ORR activity with the current normalized by the mass, in mg, of the Pd or Pt metal (mass activity) has a trend from the best to worst catalyst as follows: PtCo/C (commercial) > Pt/C (commercial) > Pd/C (TR) > Pd/C (commercial) > Pd_2Co/C (TR) > $PdCo_2$/C (TR). In the presence of methanol, the PdCo/C catalysts have better ORR activity than the Pd/C catalysts at $-2\ mA/mg_{Pd}$. A study of the kinetics and mechanism of the oxygen reduction reaction using a rotating disk electrode (RDE) and rotating ring-disk electrode (RRDE) is underway.

Table 3. Oxygen Reduction Reaction Onset Potentials at Specific Current Density as Well as Mass Activity for Our Pd/C, Pd_2Co/C, and $PdCo_2$/C and the Commercial Pd/C, Pt/C, and PtCo/C Catalysts with and without Methanol[a]

	$-0.20\ \mu A/cm^2$		$-2\ mA/mg_M$	
nanocatalysts	E (V)	E (V) w/ MeOH	E (V)	E (V) w/ MeOH
Pd/C (CRht)	0.081	0.077	0.091	0.091
Pd/C (TR)	0.121	0.122	0.114	0.094
Pd_2Co/C (TR)	0.095	0.090	0.095	0.112
$PdCo_2$/C (TR)	0.091	0.067	0.085	0.107
Pd/C commercial	0.088	0.087	0.113	0.089
Pt/C commercial	0.204		0.199	
PtCo/C commercial	0.196		0.218	

[a]All potentials are versus $Hg|Hg_2SO_4$. Current densities were determined using the electrochemical surface area. Mass activities were determined for our catalysts using the milligrams of Pd metal from the ICP−MS analysis and for the commercial catalysts using the percent metal provided by the company.

CONCLUSIONS

Three organometallic complexes were used to synthesize palladium and palladium−cobalt carbon-supported catalytic nanoparticles. The palladium−cobalt nanoparticles on Vulcan XC-72R were synthesized by chemical and thermal reduction using a single precursor with a predetermined metal ratio. The EDS, XPS, and XRD results demonstrate that the single organometallic complex can be used as precursor for the bimetallic and alloy nanocatalysts synthesis on carbon supports. The chemical reduction of the precursors gives a smaller particle size than the thermal-reduction procedure. The particle size of the carbon-supported nanoparticles increases with the incorporation of the second metal. The carbon-supported palladium nanoparticles are electroactive for the oxygen reduction reaction. The Pd_2Co/C and $PdCo_2$/C catalysts

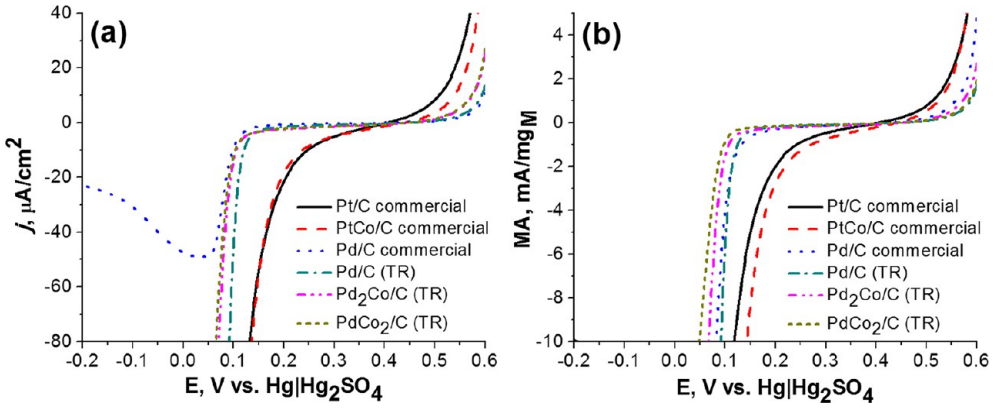

Figure 11. Oxygen reduction reaction activity normalized by (a) current density and (b) mass activity for Pt/C (straight line), PtCo/C (dashed line), and Pd/C (dotted line) commercial catalysts and our Pd/C (dash-dotted line), Pd_2Co/C (dash-dot-dotted line), and $PdCo_2/C$ (short dashed line) catalysts synthesized by thermal reduction (TR) in a 0.5 M H_2SO_4 saturated oxygen solution at scan rate of 5 mV/s.

synthesized by thermal reduction have better ORR activity than catalysts synthesized by chemical reduction. All of our catalysts have better methanol tolerance than Pt/C and PtCo/C commercial catalysts. The Pd/C and PdCo/C catalysts demonstrated that they are selective for ORR.

■ ASSOCIATED CONTENT

Supporting Information

XRD for Pd/C and $PdCo_2/C$ catalysts, STEM image and elemental line scan, SEM/EDS elemental mapping image, ORR activity and MeOH tolerance for the commercial catalysts, and BE values obtained from HR-XPS for Pd_2Co/C and $PdCo_2/C$ catalysts. This material is available free of charge via the Internet at http://pubs.acs.org.

■ AUTHOR INFORMATION

Corresponding Author

*E-mail: carlos.cabrera2@upr.edu. Tel.: 1-787-764-0000-1-4807.

Notes

The authors declare no competing financial interest.

■ ACKNOWLEDGMENTS

This research was supported in part by NASA training grant no. NNG056678H (PR Space Grant), NSF-EPSCoR Institute for Functional Nanomaterials grant no. OIA-0701525, NASA-URC grant no. NNX10AQ17A, and the Center for Education and Training in Agriculture and Related Sciences (CETARS) USDA-NIFA grant no. 2012-02177. We acknowledge Dr. Esteban Fachini for help with the XPS. We acknowledge the use of the IFN Nanoscopy Facility and Material Characterization Center (MCC) at UPR-RP, and X-Ray Diffraction and Transmission Electron Microscopy Facilities of the Cornell Center for Materials Research (CCMR).

■ REFERENCES

(1) *Fuel Cell Technology Handbook*; Hoogers, G., Ed.; CRC Press: Boca Raton, FL, 2003.
(2) EG&G Technical Services, Inc. *Fuel Cell Handbook*, 7th ed.; U.S. Department of Energy, Office of Fossil Energy, National Energy Technology: Morgantown, WV, 2004.
(3) Lima, F. H. B.; Lizcano-Valbuena, W. H.; Teixeira-Neto, E.; Nart, F. C.; Gonzalez, E. R.; Ticianelli, E. A. *Electrochim. Acta* **2006**, *52*, 385−393.
(4) Markovic, N. M.; Schmidt, T. J.; Stamenkovic, V.; Ross, P. N. *Fuel Cells* **2001**, *1*, 105−116.
(5) Wang, B. *J. Power Sources* **2005**, *152*, 1−15.
(6) Zhou, W.-P.; Yang, X.; Vukmirovic, M. B.; Koel, B. E.; Jiao, J.; Peng, G.; Mavrikakis, M.; Adzic, R. R. *J. Am. Chem. Soc.* **2009**, *131*, 12755−12762.
(7) Yang, J.; Zhou, W.; Cheng, C. H.; Lee, J. Y.; Liu, Z. *ACS Appl. Mater. Interfaces* **2010**, *2*, 119−126.
(8) Jayasayee, K.; Van Veen, J. A. R.; Manivasagam, T. G.; Celebi, S.; Hensen, E. J.M.; de Bruijn, F. A. *Appl. Catal., B* **2012**, *111*−*112*, 515−526.
(9) Brouzgou, A.; Song, S.Q.; Tsiakaras, P. *Appl. Catal., B* **2012**, *127*, 371−388.
(10) Savadogo, O.; Lee, K.; Oishi, K.; Mitsushima, S.; Kamiya, N.; Ota, K. I. *Electrochem. Commun.* **2004**, *6*, 105−109.
(11) Mustain, W. E.; Kepler, K.; Prakash, J. *Electrochim. Acta* **2007**, *52*, 2102−2108.
(12) Liu, H.; Manthiram, A. *Electrochem. Commun.* **2008**, *10*, 740−744.
(13) Mathiyarasu, J.; Phani, K. L. N. *J. Electrochem. Soc.* **2007**, *154*, B1100−B1105.
(14) Gharibi, H.; Golmohammadi, F.; Kheirmand, M. *Electrochim. Acta* **2013**, *89*, 212−221.
(15) Bezerra, C. W. B.; Zhang, L.; Liu, H.; Lee, K.; Marques, A. L. B.; Marques, E. P.; Wang, H.; Zhang, J. *J. Power Sources* **2007**, *173*, 891−908.
(16) Esmaeilifar, A.; Rowshanzamir, S.; Eikani, M. H.; Ghazanfari, E. *Energy* **2010**, *35*, 3941−3957.
(17) Antolini, E. *Appl. Catal., B* **2007**, *74*, 324−336.
(18) Karim, N.A.; Kamarudin, S. K. *Appl. Energy* **2013**, *103*, 212−220.
(19) Zeng, J.; Lee, J. Y.; Zhou, W. *J. Power Sources* **2006**, *159*, 509−513.
(20) Nitani, H.; Nakagawa, T.; Daimon, H.; Kurobe, Y.; Ono, T.; Honda, Y.; Koizumi, A.; Seino, S.; Yamamoto, T. A. *Appl. Catal., A* **2007**, *326*, 194−201.
(21) Lu, Y.; Reddy, R. G. *Electrochim. Acta* **2007**, *52*, 2562−2569.
(22) Hyun, M.-S.; Kim, S.-K.; Lee, B.; Peck, D.; Shul, Y.; Jung, D. *Catal. Today* **2008**, *132*, 138−145.
(23) Serov, A.; Nedosey, T.; Shvachko, O.; Kwak, C. *J. Power Sources* **2010**, *195*, 175−180.
(24) Hills, C. W.; Nashner, M. S.; Frenkel, A. I.; Shapley, J. R.; Nuzzo, R. G. *Langmuir* **1999**, *15*, 690−700.
(25) Nashner, M. S.; Frenkel, A. I.; Somerville, D.; Hills, C. W.; Shapley, J. R.; Nuzzo, R. G. *J. Am. Chem. Soc.* **1998**, *120*, 8093−8101.
(26) Deivaraj, T. C.; Lee, J. Y. *J. Power Sources* **2005**, *142*, 43−49.
(27) Arroyo-Ramírez, L.; Miras, H. N.; Raptis, R. G.; Cabrera, C. R. *Mater. Res. Soc. Symp. Proc.* **2010**, *1213*, T10-01.

(28) Baran, P.; Marrero, C. M.; Raptis, R.G.; Pérez, S. *Chem. Commun.* **2002**, *9*, 1012−1013.
(29) Miras, H. N.; Zhao, H.; Herchel, R.; Rinaldi, C.; Pérez, S.; Raptis, R. G. *Eur. J. Inorg. Chem.* **2008**, *2008*, 4745−4755.
(30) She, P. L.; Yao, S. B.; Zhou, S. M. *Chin. Chem. Lett.* **1999**, *10*, 407−410.
(31) Grdén, M.; Lukaszewski, M.; Jerkiewicz, G.; Czerwinski, A. *Electrochim. Acta* **2008**, *53*, 7583−7598.
(32) Trasatti, S.; Petrii, O. A. *Pure Appl. Chem.* **1991**, *63*, 711−734.
(33) Bard, A. J.; Faulkner, L. R. *Electrochemical Methods: Fundamentals and Applications*, 2nd ed.; Wiley: New York, 2001.
(34) Díaz-Ayala, R.; Arroyo-Ramírez, L.; Raptis, R. G.; Cabrera, C. R. *J. Therm. Anal. Calorim.* [Online early access] DOI: 10.1007/s10973-013-3325-7. Published Online: August **2013**.
(35) Díaz-Ayala, R.; Arroyo, L.; Raptis, R.; Cabrera, C. R. *Langmuir* **2004**, *20*, 8329−8335.
(36) Barr, T. L. *J. Phys. Chem.* **1978**, *82*, 1801−1810.
(37) Kim, K. S.; Gosmann, A. F.; Winograd, N. *Anal. Chem.* **1974**, *46*, 197−200.
(38) Kumar, S. M. S.; Herrero, J. S.; Irusta, S.; Scott, K. *J. Electroanal. Chem.* **2010**, *647*, 211−221.
(39) Joint Committee on Power Diffraction Standards (JCPDS) database card no. 46-1043.
(40) Warren, B. E. *X-ray Diffraction*; Dover Publications, Inc.: New York, 1990.
(41) Noronha, F. B.; Schmal, M.; Moraweck, B.; Delichère, P.; Brun, M.; Villain, F.; Fréty, R. *J. Phys. Chem. B* **2000**, *104*, 5478−5485.
(42) Moulder, J. F.; Stickle, W.F.; Sobol, P. E.; Bomben, K. D. *Handbook of X-ray Photoelectron Spectroscopy: A Reference Book of Standard Spectra for Identification and Interpretation of XPS Data*; Perkin-Elmer: Eden Prairie, MN, 1992.
(43) Lee, K.; Savadogo, O.; Ishihara, A.; Mitsushima, S.; Kamiya, K.; Ota, K. I. *J. Electrochem. Soc.* **2006**, *153*, A20−A24.
(44) Zhang, L.; Lee, K.; Zhang, J. *Electrochim. Acta* **2007**, *52*, 7964−7971.
(45) Zhan, L.; Lee, K.; Zhang, J. *Electrochim. Acta* **2007**, *52*, 3088−3094.
(46) Zsoldos, Z.; Guczi, L. *J. Phys. Chem.* **1992**, *96*, 9393−9400.
(47) Arroyo-Ramírez, L.; Montano-Serrano, M.; Raptis, R. G.; Cabrera, C. R. *Res. Lett. Nanotechnol.* **2009**, *2009*, 971423.
(48) Derry, G. N.; Ross, P. N. *Solid State Commun.* **1984**, *52*, 151−154.
(49) Santiago, E. I.; Varanda, L. C.; Villullas, H. M. *J. Phys. Chem. C* **2007**, *111*, 3146−3151.
(50) Fernandez, J. L.; Walsh, D.; Bard, A. J. *J. Am. Chem. Soc.* **2005**, *127*, 357−365.
(51) Liu, H.; Li, W.; Manthiram, A. *Appl. Catal., B* **2009**, *90*, 184−194.
(52) Antolini, E.; Zignani, S. C.; Santos, S. F.; Gonzalez, E. R. *Electrochim. Acta* **2011**, *56*, 2299−2305.
(53) Wagner, C. D.; Naumkin, A. V.; Kraut-Vass, A.; Allison, J. W.; Powell, C. J.; Rumble, J. R. *NIST X-ray Photoelectron Spectroscopy Database*, version 3.5; U.S. Department of Commerce: Gaithersburg, MD, 2007.
(54) Tominaka, S.; Momma, T.; Osaka, T. *Electrochim. Acta* **2008**, *53*, 4679−4686.
(55) Yi, Q.; Niu, F.; Sun, L. *Fuel* **2011**, *90*, 2617−2623.